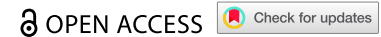


ORIGINAL RESEARCH



## XL888 and pembrolizumab modulate the immune landscape of colorectal tumors in a phase Ib/II clinical trial

Maggie J. Phillips<sup>a\*</sup>, Olatunji B. Alese<sup>a\*</sup>, Natalie K. Horvat<sup>a</sup>, Emily Greene<sup>a</sup>, Olumide B. Gbolahan<sup>a</sup>, Kathleen Coleman<sup>b</sup>, Deon B. Doxie<sup>b</sup>, Vaunita Parihar<sup>b</sup>, Zaid K. Mahdi<sup>c</sup>, Ashley McCook-Veal<sup>d</sup>, Jeffrey M. Switchenko<sup>d</sup>, Maria Diab<sup>e</sup>, Cameron J. Herting<sup>a</sup>, Chrystal M. Paulos<sup>f,g</sup>, Bassel F. El-Rayes<sup>h#</sup>, and Gregory B. Lesinski<sup>a#</sup>

<sup>a</sup>Department of Hematology and Medical Oncology, Emory University, Atlanta, GA, USA; <sup>b</sup>Winship Cancer Institute of Emory University, Atlanta, GA, USA; <sup>c</sup>Department of Pathology, Emory University, Atlanta, GA, USA; <sup>d</sup>Department of Biostatistics & Bioinformatics, Emory University, Atlanta, GA, USA; <sup>e</sup>Department of Internal Medicine, Henry Ford Hospital, Detroit, MI, USA; <sup>f</sup>Department of Surgery, Emory University, Atlanta, GA, USA; <sup>g</sup>Department of Microbiology and Immunology, Emory University, Atlanta, GA, USA; <sup>h</sup>Department of Medicine, University of Alabama at Birmingham, Birmingham, AL, USA

### ABSTRACT

We conducted a phase Ib/II clinical trial to evaluate the safety, feasibility, and clinical activity of combining pembrolizumab (anti-PD-1) with XL888 (Hsp90 inhibitor) in patients with advanced colorectal cancer (CRC). We hypothesized that this regimen would modulate soluble and cellular immune mediators and enhance clinical outcomes. The trial employed a 3 + 3 open-label design, with an expansion cohort at the recommended phase II dose (RP2D) in treatment-refractory, mismatch repair-proficient CRC patients. Comprehensive analyses of plasma cytokines, peripheral blood mononuclear cells (PBMCs), and spatial immune cell patterns in liver biopsies were performed to identify unique immune signatures resulting from the combined therapy. The combination of pembrolizumab and XL888 proved to be safe and feasible, with a subset of patients achieving stable disease, although no objective responses were observed in this heavily pre-treated population. Correlative studies revealed immunomodulatory effects in tumors and circulation, including a reduction in IL6<sup>+</sup> cells and macrophages (CD68<sup>+</sup>) within metastatic liver tissue, alterations in blood CD3<sup>+</sup> cells, and upregulation of numerous inflammatory plasma cytokines. These findings suggest local and systemic immune activation by the combination of pembrolizumab and XL888. While clinical activity was modest in treatment-refractory CRC patients, there were notable effects on the tumor immune environment and systemic immune modulation.

### ARTICLE HISTORY

Received 4 November 2024  
Revised 17 February 2025  
Accepted 2 March 2025

### KEYWORDS





Clinical trial; colorectal cancer; cytokines; heat shock protein; immune checkpoint inhibitors; immunotherapy

## Introduction


Colorectal cancer (CRC) is the third most common cause of cancer-related death among men and women in the United States. It is projected to be the leading cause of death by 2040.<sup>1,2</sup> Notably, half of patients diagnosed with early-stage CRC progress to metastatic disease.<sup>3</sup> Surgery remains a standard of care for patients with early-stage or limited metastatic CRC, contributing to more favorable survival outcomes.<sup>4</sup> However, despite advances in systemic therapy for CRC, the 5-year survival rate for patients with advanced disease remains bleak (15–25%).<sup>5</sup> While immune checkpoint inhibitors (ICIs) show efficacy in CRC patients with deficient mismatch repair (dMMR) or high microsatellite instability (MSI-H), these individuals constitute a minority (~5%) of advanced CRC cases.<sup>6,7</sup> Additional treatment options are urgently needed for most CRC patients. Recent studies with Fc-enhanced cytotoxic T-lymphocyte-associated protein-4 (CTLA-4) antibody

blockade combinations offer hope that immunotherapy remains a viable approach.<sup>8</sup> Considerable efforts are ongoing to modulate features of the immune tumor landscape as a potential means to improve the effectiveness of ICIs, such as antibodies targeting programmed cell death-1 (PD-1). Ultimately, by targeting other components of the tumor microenvironment (TME), it may be possible to broaden the scope of immunotherapy to patients with proficient mismatch repair (pMMR) or microsatellite stable (MSS) tumors.

Inhibition of Hsp90, a chaperone protein crucial for cellular stress responses, has shown promise due to its dual capacity to elicit tumor cell apoptosis and modulate the immune milieu of cancers.<sup>9,10</sup> Evidence from preclinical studies indicates Hsp90 inhibitors (Hsp90i) may harbor a unique mechanism of action by altering components of tumor stroma. For example, XL888, a synthetic small-molecule inhibitor that binds to the ATP pocket in the N-terminus of

**CONTACT** Bassel El-Rayes  [belrayes@uabmc.edu](mailto:belrayes@uabmc.edu)  Division of Hematology and Oncology, Department of Medicine, O'Neal Comprehensive Cancer Center, University of Alabama at Birmingham Heersink School of Medicine, 1670 University Blvd., Birmingham, AL, 35233 USA; Gregory B. Lesinski  [gregory.b.lesinski@emory.edu](mailto:gregory.b.lesinski@emory.edu)  Department of Hematology and Medical Oncology, Winship Cancer Institute of Emory University, 1365 Clifton Rd. NE, Atlanta, GA 30322, USA

\*Denotes Equal Contribution.

 Supplemental data for this article can be accessed online at <https://doi.org/10.1080/2162402X.2025.2475620>

© 2025 The Author(s). Published with license by Taylor & Francis Group, LLC.

This is an Open Access article distributed under the terms of the Creative Commons Attribution-NonCommercial License (<http://creativecommons.org/licenses/by-nc/4.0/>), which permits unrestricted non-commercial use, distribution, and reproduction in any medium, provided the original work is properly cited. The terms on which this article has been published allow the posting of the Accepted Manuscript in a repository by the author(s) or with their consent.

Hsp90, reduced IL-6 secretion and restricted growth of pancreatic-derived cancer-associated fibroblasts (CAFs) *in vitro*.<sup>11–13</sup> Combined XL888 and anti-PD-1 in murine pancreatic cancer models increased tumor infiltrating lymphocytes (TIL), induced immune response genes, and enhanced efficacy of anti-PD-1 therapy. Furthermore, when combined with anti-PD-1, Hsp90i limited tumor growth in mice, with increased effector lymphocytes and decreased suppressive immune cell populations detected in these animals.<sup>13</sup> The availability of clinically viable Hsp90i, like XL888, provides an approach to target solid tumors and modulate their associated immune and stromal components.

Hsp90 plays a crucial role in folding protein and maintaining protein function involved in inflammatory signaling pathways, including JAK/STAT family members and HIF-1 $\alpha$ . Activation of HIF-1 $\alpha$  and the JAK-STAT pathway increases immune-suppressive proteins, including programmed death-ligand 1 (PD-L1).<sup>14–16</sup> CRC patients receiving ganetespib, an Hsp90i, displayed less HIF-1 $\alpha$  and JAK-STAT.<sup>17</sup> Therefore, targeting Hsp90 may also modulate immune inhibitory pathways including PD-1/PD-L1.

We hypothesized that Hsp90 inhibition could be safely combined with antibodies targeting PD-1 in patients with advanced gastrointestinal malignancy. We also posited that it would favorably modulate the TME to improve immune function and potentiate the effects of PD-1 inhibitors in patients with advanced CRC. In this report, we describe results from a first-in-human phase 1b trial evaluating the safety of combining XL888 with pembrolizumab and a phase 2 expansion cohort in patients with stage IV treatment – refractory pMMR CRC, along with associated laboratory correlative studies.

## Materials and methods

### Study design and participants

The trial design included patients with advanced or metastatic gastrointestinal adenocarcinomas, such as esophagogastric, cholangiocarcinoma, hepatocellular, pancreatic, small bowel, or colorectal cancers, with documented progression after at least one prior therapy. In the expansion phase, patients with colorectal cancer were enrolled if they had pMMR, treatment-refractory disease, defined as previously treated with oxaliplatin, irinotecan, and a fluoropyrimidine. Patients were also required to have measurable disease per RECIST version 1.1, with an Eastern Cooperative Oncology Group (ECOG) performance status (PS) of 0, 1 or 2. Required laboratory cutoff values were as follows: absolute neutrophil count  $\geq 1500/\mu\text{L}$ , platelets  $\geq 100 \times 10^9/\text{L}$ , hemoglobin  $\geq 90 \text{ g/L}$ , serum creatinine  $\leq 1.5 \times$  upper limit of normal (ULN), serum total bilirubin  $\leq 1.5 \times$  ULN, and serum albumin  $\geq 2.5 \text{ mg/dL}$ . Key exclusion criteria included the following: diagnosis of immunodeficiency, or use of systemic steroid therapy or any other form of immunosuppressive therapy within 7 days prior to the first dose of trial treatment. Patients

receiving prior therapy with an anti-PD-1, anti-PD-L1, or anti-PD-L2 agent were excluded. Additionally, history or evidence of retinal pathology on ophthalmologic examination that is considered a risk factor for neurosensory retinal detachment, RVO (retinal vein occlusion), or neovascular macular degeneration were excluded. The study protocol was reviewed and ethically approved by the Emory University Institutional Review Board (IRB; IRB00087397). Patients granted written consent prior to any screening activities or data collection. The Winship Data and Safety Monitoring Board (DSMB) gave additional oversight through biannual monitoring and reviewed the safety and efficacy findings. The clinical trial was registered with clinicaltrials.gov (NCT03095781).

### Clinical procedures

Patients were treated with pembrolizumab (200 mg) via intravenous (IV) infusion on day 1 and XL888 orally twice weekly in 21-day cycles until disease progression, unacceptable toxicity, or patient preference to discontinue. Study participation ranged from early withdrawal before the initial scan at cycle 1 day 3 (C1D3) to completing six cycles. Dose-escalation tested XL888 at 45 mg (DL1), 90 mg (DL2), and 60 mg (DL3, if  $\geq 1$  DLTs at DL2). Without dose-limiting toxicity (DLTs), the study expanded to enroll 16 additional CRC patients meeting eligibility criteria. Patients receiving  $<80\%$  of prescribed doses for non-toxicity reasons were deemed unevaluable for the primary endpoint and replaced.

In the expansion phase, patients were assigned to pembrolizumab or pembrolizumab with XL888, with all receiving combination therapy after 3 weeks. The expansion phase aimed to confirm safety and collect biomarker samples. Serial blood was collected on cycle 1 day 1 (C1D1) and cycle 1 day 15 (C1D15), with paired metastatic biopsies obtained from 4 patients in each treatment group. Safety data was tabulated, by type and grade, while Kaplan–Meier curves estimated progression-free survival (PFS) and overall survival (OS).

### Study endpoints

The primary endpoint was safety and toxicity of the combination therapy, defined at the recommended phase II dose (RP2D) of pembrolizumab, administered with XL888. Standard definitions of dose limiting toxicities were applied. Secondary endpoints were PFS, OS, duration of response (DoR), and objective response rate (ORR). Response duration was defined as the time from the participant's first documented response until disease progression. ORR was defined as complete response (CR) or partial response (PR) as best response on the study, as determined by RECIST version 1.<sup>18,19</sup> Radiographic and clinical evaluations were performed every 8 weeks during treatment and at study end when possible. Treatment continued until disease progression or withdrawal. All serious adverse events (AEs) and treatment-related grade 3–5 AEs were reported using CTCAE v4.0

### Correlative translational studies

Peripheral blood was collected at C1D1 and C1D15 from patients ( $n = 14$ ) receiving pembrolizumab with XL888 in the dose-escalation phase (Figure 1). For CRC dose-expansion patients ( $n = 16$ ), blood and biopsies were collected at both time points. Correlative analyses were performed on specimens from all 18 CRC patients receiving either pembrolizumab alone ( $n = 7$ ) or combined with XL888 at RP2D ( $n = 11$ ).

### Procurement of metastatic liver tissue for correlative studies

Eight CRC patients (pembrolizumab,  $n = 4$ ; pembrolizumab/XL888,  $n = 4$ ) underwent image-guided core needle biopsies of metastatic liver tissue at C1D1 and C1D15, at the same metastatic site. Initial biopsy acquisition occurred upon enrollment, after a two-week treatment-free interval. One to four biopsies were obtained per patient from the same metastatic site, excluding bone metastases. One core was formalin-fixed for multiplex immunohistochemistry (mIHC), while additional cores, were processed fresh for immediate single-cell mass cytometry (CyTOF) analysis.

### Metastatic liver mIHC and analysis

Tissue biopsies were fixed in 10% buffered formalin phosphate and embedded in paraffin. Sections of 4  $\mu\text{m}$  thickness were cut and mounted onto slides. The multiplex immunohistochemistry (mIHC) staining protocol was carried out using the DISCOVERY ULTRA autostainer (Roche Diagnostics). Two distinct staining panels were utilized: panel 1 targeted markers including  $\alpha$ -SMA, CD3, CD19, CD68, IL6, CK19, and DAPI, while panel 2 included CD4, CD8, CK19, FoxP3, ROR $\gamma$ t, T-bet, and DAPI. After staining, the slides were cover-slipped with mounting medium and allowed to cure before imaging with the Vectra<sup>®</sup> Polaris<sup>™</sup> Automated Quantitative Pathology Imaging System. The cured slides containing fluorescently labeled tissue sections underwent whole-slide scanning and subsequent analysis using QuPath v0.4.4.4 (University of Edinburgh, Edinburgh, Scotland, UK).<sup>20</sup> Refer to Appendix 1 and Supplementary Table S1 for comprehensive details on the mIHC staining protocol and marker information.

### Metastatic liver digestion, CyTOF, and analysis

Fresh metastatic liver tissue cores were subjected to both mechanical and enzymatic dissociation processes using the

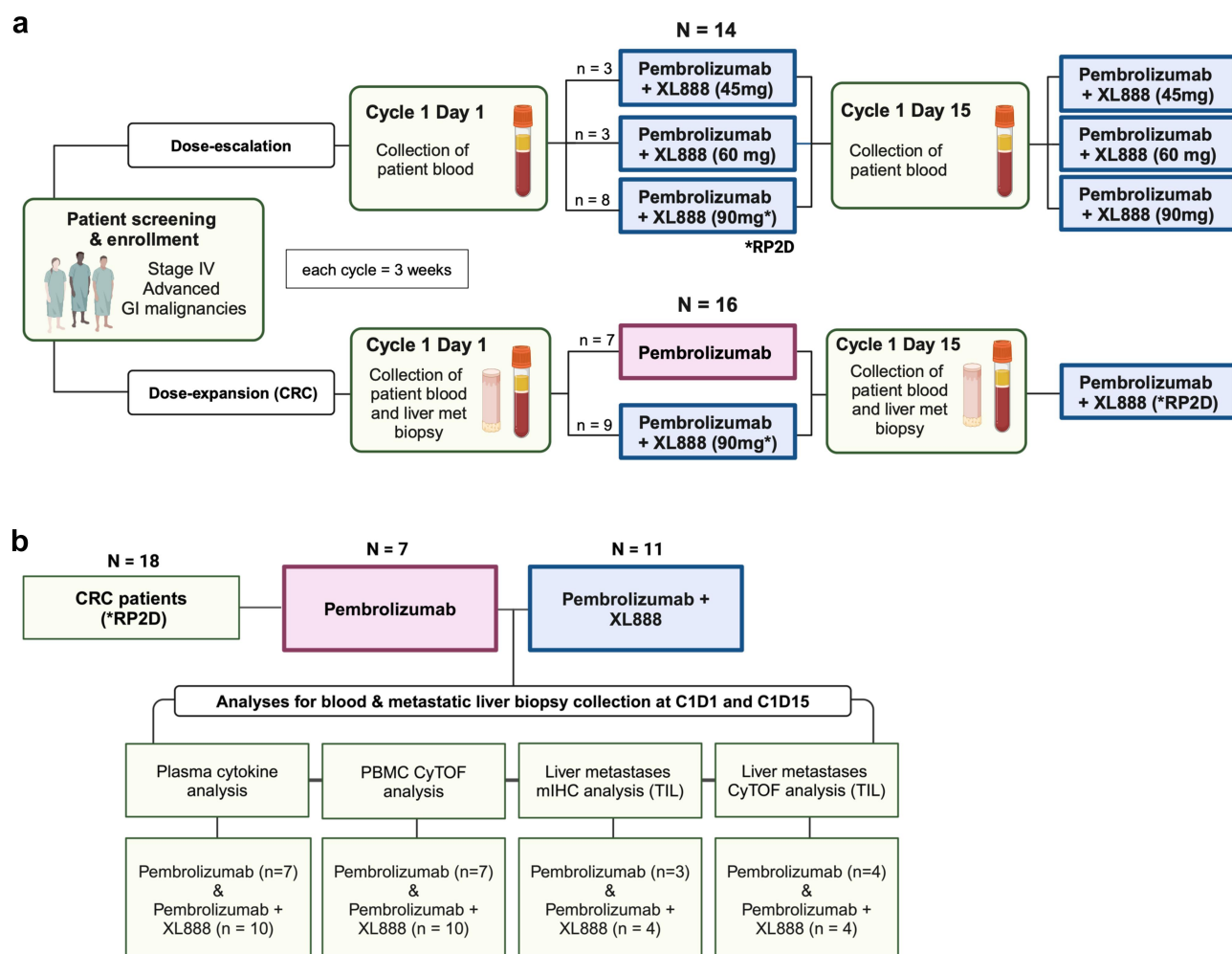


**Figure 1.** Peripheral blood and metastatic liver biopsy collection timeline for correlative studies. (a) Timeline examines blood and biopsy collection timepoints during cycle 1 for the dose-escalation and colorectal cancer (CRC) dose-expansion phases of the trial. (b) Schematic displays CRC patients receiving the RP2D, detailing analyses performed and the total number of samples processed for each analysis. Images created using BioRender.com.

gentleMACS Dissociator (catalog# 130-093-235, Miltenyi Biotec). For a comprehensive description of the tumor dissociation and digestion process, refer to [Appendix 2](#). The dissociation procedure yielded approximately  $2 \times 10^6$  cells or fewer per sample for CyTOF analysis.

Cells from dissociated metastatic liver tissue were stained for viability using Cell-ID™ Cisplatin (catalog# 201064, Standard BioTools) in 1X PBS, followed by surface and intracellular staining with Maxpar® Cell Staining Buffer and fixation in 1.6% formaldehyde. Samples were then labeled with Cell-ID™ Intercalator-Ir (catalog# 201192A, Standard BioTools) and acquired on a Helios mass cytometer; detailed protocols and antibody lists can be found in [Appendix 3](#) and Supplementary Table S2, respectively. The Flowjo V10.8.1 and Cytobank software were used to analyze normalized CyTOF FCS files.

## Peripheral blood processing and analyses

### Plasma cytokine analysis

Peripheral blood specimens were collected in EDTA tubes at C1D1 and C1D15. Plasma was isolated from whole blood and stored at  $-80^{\circ}\text{C}$ . Samples were analyzed using the Human Cytokine/Chemokine Panel, a 48-plex Discovery Assay® Array (Eve Technologies), which employs Luminex™ laser bead technology. Undiluted plasma samples were analyzed in duplicate, with final concentrations reported in pg/mL. For details on specific analytes and processing methods, refer to Supplementary Table 3 and [Appendix 4](#), respectively. Notably, one patient was excluded from the analyses due to the absence of a blood draw at C1D15.

### Whole blood MaxPar™ Direct Immune Profiling Assay (MDIPA)

PBMCs were isolated from whole blood using Ficoll® density gradient centrifugation at  $800 \times g$  for 30 min. Isolated PBMCs were cryopreserved in Serum-Free Cell Freezing Medium with DMSO (Sigma-Aldrich). Samples were acquired on a Helios mass cytometer (Standard Biotoools) and analyzed using MDIPA and Maxpar PathSetter software version 2.0.45. For a list of identified cellular markers consult Supplementary Table 4, and [Appendix 5](#) for the detailed protocol.

## Statistical considerations

### Clinical

The 3 + 3 standard phase I trial design was used for the dose-escalation phase, evaluating 45 mg and 90 mg cohorts, with a potential 60 mg intermediate if  $\geq 2$  DLTs were observed in the 90 mg cohort. The expansion phase began after establishing the RP2D. A sample size of 16 patients was based on a 20% ORR endpoint for XL888 and pembrolizumab combination, with a null response rate of 2% ( $\alpha = 0.1$ , power = 80%). AEs were summarized by frequencies and percentages. SAS 9.4 (SAS Institute Inc.) was used for statistical analysis. Categorical variables were summarized by frequencies and percentages, and continuous variables by median and IQR. PFS and OS were estimated using the Kaplan–Meier method.

## Correlative studies

Changes in biomarkers from C1D1 to C1D15 were assessed using the Wilcoxon matched pairs signed rank test. This was applied to both treatment groups (pembrolizumab alone and combined with XL888), comparing paired C1D1 and C1D15 measurements. These time points were chosen to ensure analysis could be conducted on the greatest number of patients prior to disease progression. Differences were considered statistically significant at  $p < 0.05$ .

## Results

### Safety, efficacy outcomes, and demographics for phase I dose-escalation

Fourteen patients were enrolled on the dose-escalation portion of the trial, as detailed in [Table 1](#). Their median age was 66.5 years (IQR 59–71), with more male patients enrolled (64%). Diagnoses included CRC ( $n = 5$ ), pancreatic adenocarcinoma (PDAC;  $n = 6$ ), biliary tract (BTC;  $n = 1$ ), ampullary ( $n = 1$ ), and duodenal ( $n = 1$ ) cancers. All patients had discontinued treatment at data cutoff. Two patients were ineligible for assessing the primary endpoint (RP2D) due to biliary stent obstruction and sepsis. One dose-limiting

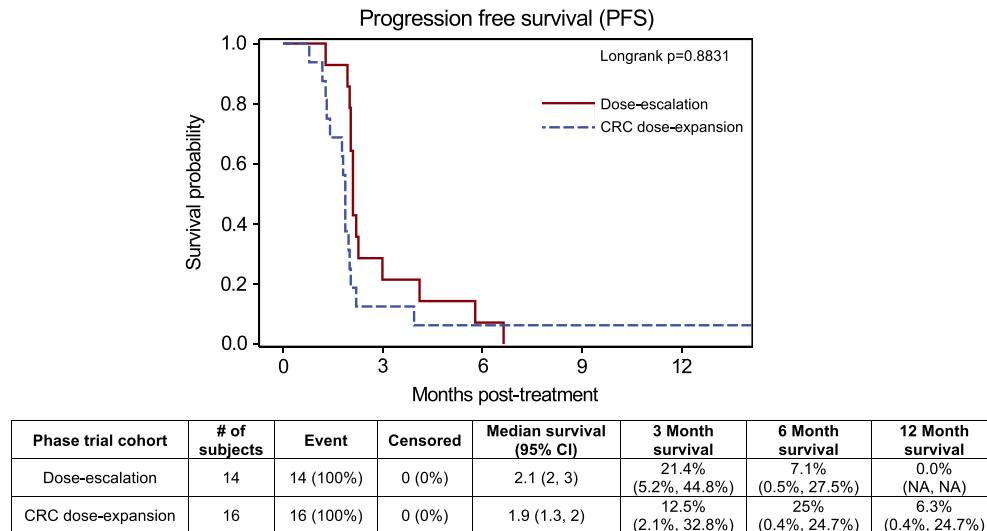
**Table 1.** Demographic information for participants, separated by dose-escalation and colorectal cancer (CRC) dose-expansion cohort.

Patient demographics by cohort	
<b>Dose-escalation cohort</b>	
<b>N = 14</b>	
<b>Cancer diagnosis</b>	
Colorectal cancer (CRC), RP2D = 2	6
Pancreatic ductal adenocarcinoma (PDAC)	5
Biliary tract cancer (BTC)	1
Ampullary	1
Duodenal	1
<b>Sex</b>	
Female	5
Male	9
<b>Race/ethnicity</b>	
Caucasian	13
African American	1
<b>Age</b>	
Median age	66.5
Interquartile range	59–71
<b>Prior therapies</b>	
1	2
2	5
3 or more	7
<b>CRC dose-expansion cohort</b>	
<b>N = 16</b>	
<b>Cancer diagnosis</b>	
Colorectal cancer (CRC), RP2D = 16	16
<b>Sex</b>	
Female	9
Male	7
<b>Race/ethnicity</b>	
Caucasian	13
African American	3
<b>Age</b>	
Median age	56.5
Interquartile range	50–63
<b>Prior therapies</b>	
1	2
2	5
3 or more	9

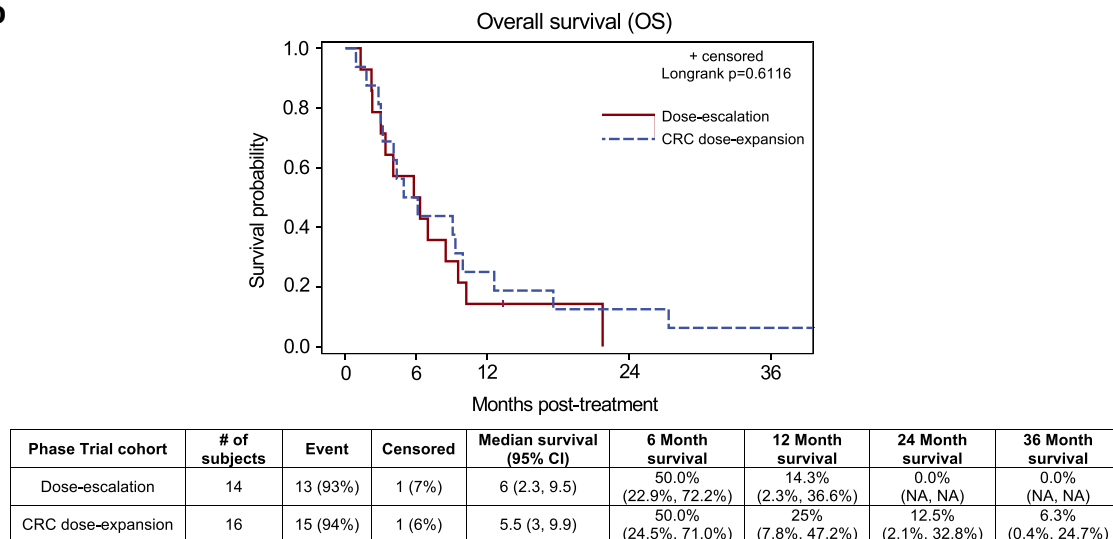
toxicity (DLT) (grade 3 [G3] autoimmune hepatitis) was observed on DL2 (pembrolizumab 200 mg + XL888 90 mg). We therefore enrolled three patients on DL3 (pembrolizumab 200 mg + XL888 60 mg). No DLT was observed, and five additional patients were subsequently enrolled on DL2 with no additional DLT. Three patients (1 duodenal, 2 CRC) had prolonged stable disease (6, 9 and 15 cycles,

respectively). Median PFS for patients in the dose escalation phase was 2.1 months (95% CI, 2–3 months; Figure 2(a)) and median OS was 6 months (95% CI, 2.3 to 9.5 months; Figure 2(b)). The most common treatment-related toxicities included autoimmune hepatitis (G3;  $n = 1$ ), retinopathy (G2;  $n = 2$ ), nausea (G2;  $n = 1$ ), constipation (G2;  $n = 1$ ), and diarrhea (G2;  $n = 6$ ) (Supplementary Table 5).

**a**



**b**



**c**

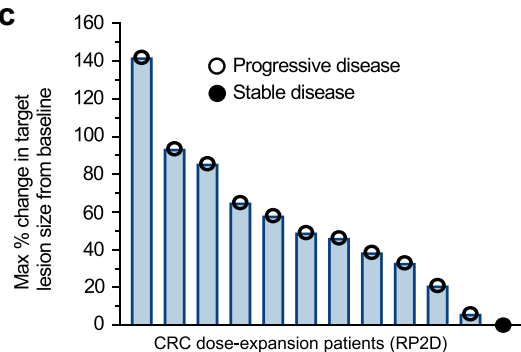


**Figure 2.** Clinical outcomes for patients in the dose-escalation and CRC dose-expansion phases. a-b Kaplan-Meier plots display the PFS (a) and OS (b) outcomes for patients in the dose-escalation and CRC-expansion phase of the trial. (c) Maximum percent change in the size of target metastatic liver lesions from baseline for the CRC dose-expansion phase. Each bar represents an individual patient.

### Safety, efficacy outcomes, and demographics for CRC phase I dose-expansion

Sixteen patients with CRC were subsequently enrolled and treated at the RP2D (pembrolizumab 200 mg + XL888 90 mg) (Table 1). The median age in the expansion cohort was 56.5 years (IQR range 50–63). Those on study were quite advanced, as all patients enrolled had received at least two prior lines of systemic treatment for metastatic disease. Most patients had left-sided tumors ( $n = 11$ ; 68%). Twelve patients had a tumor with RAS mutation, 1 with BRAF mutation, and 14 were mismatch repair proficient (pMMR) (Supplementary Table 6). All patients were eligible and evaluable for safety, ORR, PFS, and OS analyses. There was no objective response in the study population, but 4 (25%) patients had stable disease (SD) as the best response on treatment. Overall, median PFS was 1.9 months (95% CI, 1.3 to 2 months; Figure 2(a)) and median OS was 5.5 months (95% CI, 3 to 9.9 months; Figure 2(b)). Figure 2(c) illustrates the maximum percent change in size of target metastatic liver lesion from baseline. Among the 16 patients in the dose-expansion cohort, two experienced progressive disease (PD) and could not be assessed due to treatment discontinuation, while the percent change for two other patients remains unavailable.

Grade 3–4 AEs and SAEs (at least possibly related to pembrolizumab combined with XL888 treatment) were reported in 12.5% of patients included in the safety analysis. These parameters included myocarditis ( $n = 1$ ), periorbital edema ( $n = 1$ ), retinopathy ( $n = 1$ ), diarrhea ( $n = 1$ ), nausea/vomiting ( $n = 1$ ), and increased liver enzymes (Alanine aminotransferase [ALT] and Aspartate aminotransferase [AST];  $n = 1$ ) (Table 2). No Grade 5 AEs were reported. The most common AEs (any grade) were diarrhea (46.7%), fatigue (40%), abdominal pain (20%), constipation, nausea, vomiting, eye disorders, Alkaline phosphatase (Alk P) increased, AST increased, ALT increased, anorexia, hypomagnesemia, and cough (16.7% each) (Supplementary Table 5).

### IL6<sup>+</sup> cells and CD68<sup>+</sup> macrophage populations are reduced in CRC liver metastases treated with pembrolizumab and XL888

These correlative studies provide insights into the immune modulatory effects of Hsp90 inhibition, potentially leading to

innovative combination strategies with ICI therapy. We analyzed paired metastatic liver biopsies (C1D1, C1D15) from CRC patients receiving either pembrolizumab alone ( $n = 3$ ) or combined with XL888 ( $n = 4$ ). Through mIHC (panel 1, Figure 3(a)), we observed fewer IL6<sup>+</sup> cells in CRC tumors treated with pembrolizumab combined with XL888 (Figure 3(b)). In contrast, there was a trend toward more overall IL-6<sup>+</sup> cells in tumors from patients treated with pembrolizumab alone. No impact of treatment was observed on the frequency of  $\alpha$ -SMA<sup>+</sup> cells, a marker of activated cancer-associated fibroblasts (CAFs), and  $\alpha$ -SMA<sup>+</sup>IL-6<sup>+</sup> cells (Supplementary Figure S1A and Figure 3(c), respectively). However, tumors from combination treatment patients showed a trending decrease in CD68<sup>+</sup> (Figure 3(d)) and CD68<sup>+</sup>IL6<sup>+</sup> macrophages (Figure 3(e)). No significant differences were observed in other immune cells, including CD19<sup>+</sup> and CD3<sup>+</sup>, between treatment groups or cycle days (Supplementary Figure S1A). T cell population changes were inconclusive due to low cell detection (panel 2, Supplementary Figure S1B–C). Spatial analysis on mIHC examined immune and stromal cell distribution patterns relative to tumor margins and stromal compartment (Supplementary Figure S2A–B). We quantified  $\alpha$ -SMA<sup>+</sup>, CD68<sup>+</sup>, and CD3<sup>+</sup> cells' spatial location (Supplementary Figures S3 and 4) but observed no significant changes between C1D1 and C1D15 in either treatment group. Other cell populations showed no differences, possibly due to cell abundance, tissue quality, and/or patient heterogeneity.

### CyTOF reveals CD19<sup>+</sup> lymphocytes are decreased in CRC patients treated with pembrolizumab and XL888

We used CyTOF to analyze lymphocyte populations in paired metastatic liver biopsies (C1D1, C1D15) from CRC patients receiving pembrolizumab alone ( $n = 4$ ) or combined with XL888 ( $n = 4$ ). Due to limited cell abundance and tissue quality, conclusive analysis of most immune cell populations, including CD4 and CD8 T cells, was challenging (Supplementary Figure S5A–C). However, we observed a trend of fewer CD19<sup>+</sup> cells in biopsies from patients receiving pembrolizumab combined with XL888 (Figure 4(a–b)).

### Systemic increase in inflammatory cytokines observed in response to pembrolizumab and XL888

We investigated plasma cytokine, chemokine, and growth factor profiles of CRC patients treated with pembrolizumab alone ( $n = 7$ ) or combined with XL888 ( $n = 10$ ) to assess systemic immune effects. Comparing C1D1 to C1D15, IL-6 concentration was approximately two-fold higher in patients receiving the combination therapy ( $p = 0.0075$ ) (Figure 5(a)). Significant increases were observed in several inflammatory factors for the combination group, including IL-6 ( $p = 0.0020$ ), IP-10 ( $p = 0.0020$ ), MCP-1 ( $p = 0.0059$ ), MDC ( $p = 0.0488$ ), IL-15 ( $p = 0.0195$ ), and Eotaxin ( $p = 0.0273$ ) (Figure 5(b)). Pembrolizumab alone showed similar trends, though only IL-1RA increased significantly ( $p = 0.0312$ ). Other cytokine levels showed no trends or had low concentrations (Supplementary Figure S6).

**Table 2.** Treatment-related grade 3–4 adverse events observed in patients receiving combined pembrolizumab and XL888.

Adverse Events	Grade 3–4
Any	6 (14.6)
Cardiac disorders	1 (2.4)
Atrioventricular block complete	1 (2.4)
Myocarditis	1 (2.4)
Eye disorders	2 (4.9)
Periorbital edema	1 (2.4)
Retinopathy	1 (2.4)
Gastrointestinal disorders	2 (4.9)
Diarrhea	1 (2.4)
Nausea	1 (2.4)
Vomiting	1 (2.4)
Immune system disorders	1 (2.4)
Autoimmune disorder	1 (2.4)
Alanine aminotransferase increased	1 (2.4)
Aspartate aminotransferase increased	1 (2.4)
Cardiac troponin I increased	1 (2.4)

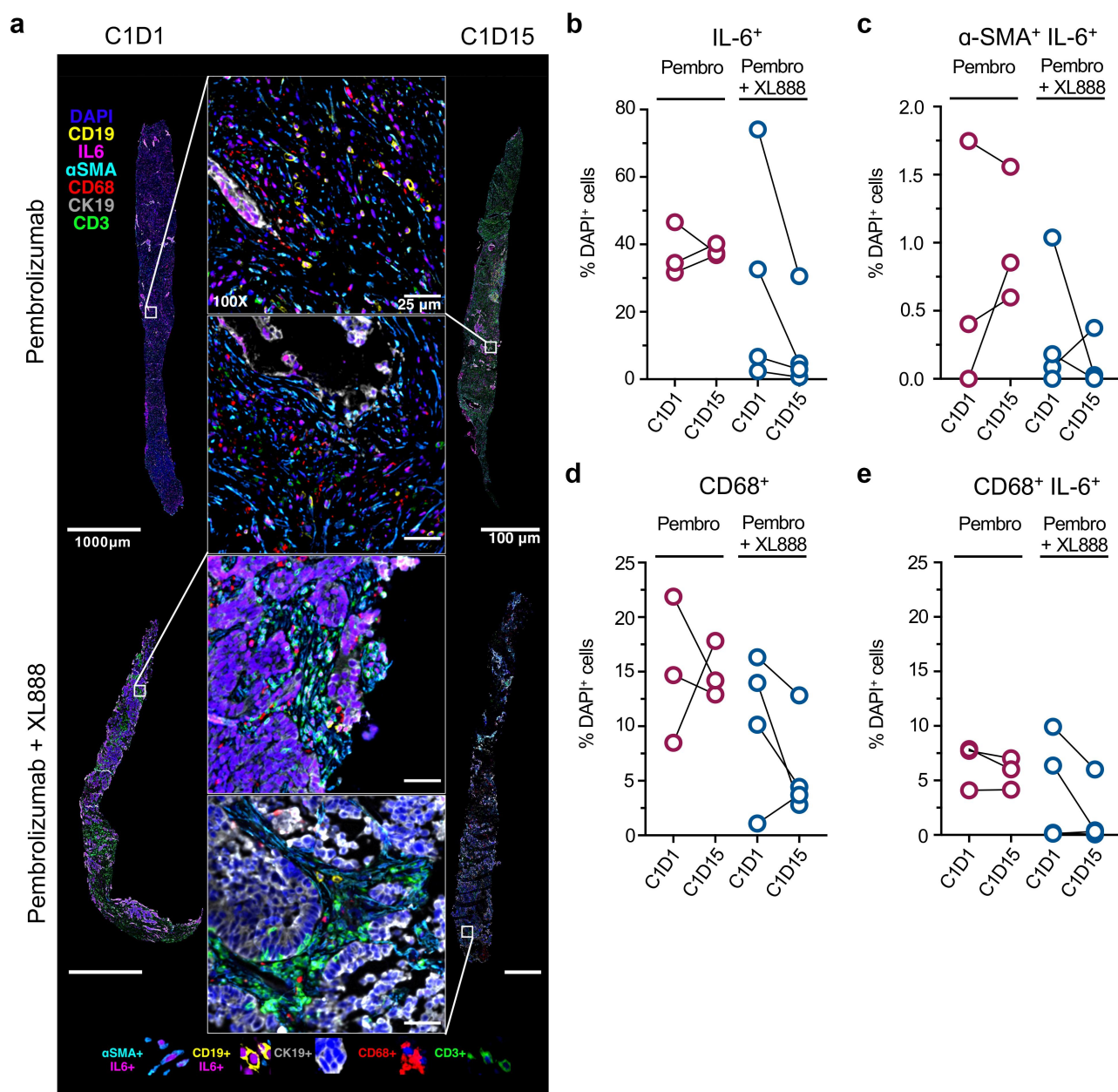


**Figure 3.** Multiplex immunohistochemistry (mIHC) analysis of immune and stromal cell populations in paired metastatic liver biopsies at C1D1 and C1D15 with pembrolizumab alone or combined with XL888. (a) Representative mIHC image of paired liver biopsies. Specific biomarkers displayed for panel 1 include, DAPI (royal blue), CD19 (yellow), IL-6 (magenta), α-SMA (light blue), CD68 (red), CK19 (gray), and CD3 (green) as indicated in the top left; white scale bars represent 25 μm, 100 μm, or 1000 μm. b-e. Percentage of IL-6<sup>+</sup> (b), α-SMA<sup>+</sup> IL-6<sup>+</sup> (c), CD68<sup>+</sup> (d), and CD68<sup>+</sup> IL-6<sup>+</sup> (e) as a proportion of DAPI<sup>+</sup> cells.

To note, one patient from the combination group was excluded from analysis, due to missing a blood draw at C1D15.

#### **Systemic alterations were evident in certain immune cell populations, including CD3<sup>+</sup> T cells, in patients following combined pembrolizumab and XL888 treatment**

To assess potential peripheral cellular changes alongside our systemic data, we analyzed patient PBMCs using CyTOF with a 30-marker immune panel. In patients receiving combined therapy, we detected a trend toward fewer circulating total CD45<sup>+</sup> leukocytes after treatment, though this was not significant (Figure 6(a)). Notably, the proportion of circulating CD3<sup>+</sup> T cells was significantly lower compared to baseline

( $p = 0.0273$ ) (Figure 6(b)). The proportion of CD8<sup>+</sup> T cells remained stable from C1D1 to C1D15 (Figure 6(c)), while CD4<sup>+</sup> T cells trended lower, but without statistical significance (Figure 6(d)). Additionally, no discernible patterns were observed in the proportions of CD4<sup>+</sup> and CD8<sup>+</sup> cells relative to CD3<sup>+</sup> T cells (Supplementary Figure 7). Other immune populations analyzed from the MDIPA panel showed no significant differences (data not shown).

#### **Discussion**

This study is the first to report the clinical and correlative data outcomes of patients with advanced gastrointestinal malignancies treated with the novel combination of

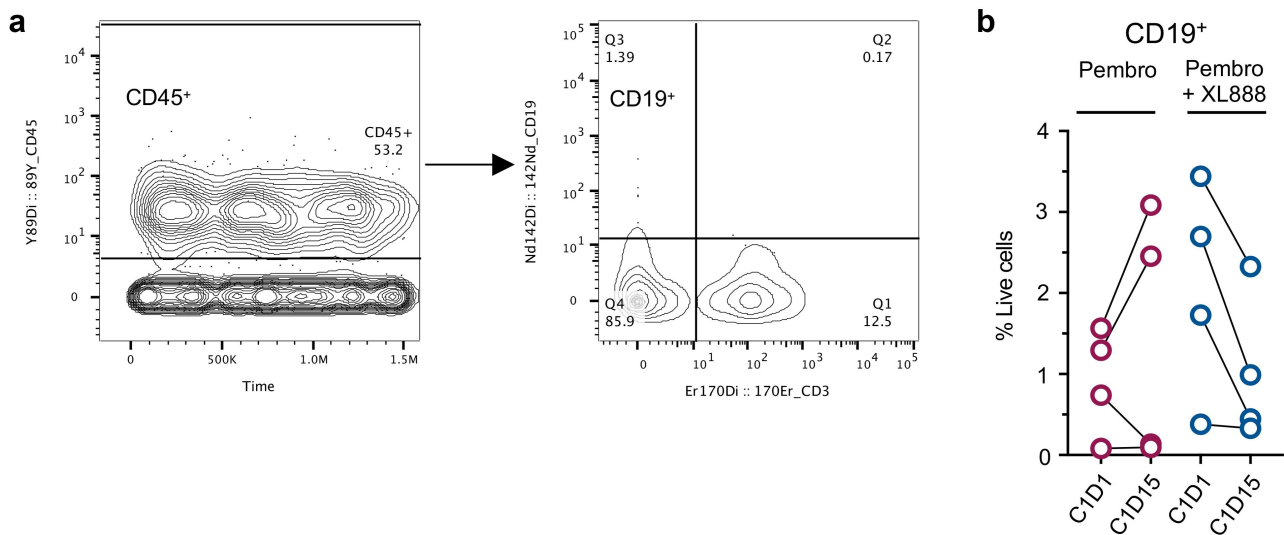


**Figure 4.** CyTOF-based identification and quantification of CD19<sup>+</sup> cells in liver metastases at C1D1 and C1D15 in patients treated with pembrolizumab alone or in combination with XL888. (a) CyTOF gating strategy demonstrating the sequential identification of CD45<sup>+</sup> cells followed by CD19<sup>+</sup> cells within the gated population. (b) Percentage of live CD19<sup>+</sup> cells from C1D1 to C1D15 in patients treated with pembrolizumab ( $n = 4$ ) or in combination with XL888 ( $n = 4$ ).

pembrolizumab and XL888. This trial was inspired by our prior pre-clinical data in mice showing XL888 can operate via an unacknowledged mechanism involving reduced activation of CAFs and concomitant reduction of IL-6. These studies further showed in murine models of pancreatic cancer, that the combination of XL888 and PD-1 blockade could elicit antitumor efficacy mediated by CD8<sup>+</sup> T cells.<sup>12</sup> This ability to potentiate immunotherapy in the pre-clinical setting was reproducible when other Hsp90i were used. For example, inhibiting Hsp90 using ganetespib can modulate angiogenesis, inhibit tumor invasion, and induce cytokines (i.e. VEGF, MIF) and inflammatory pathways such as NF- $\kappa$ B.<sup>17,21–23</sup> Finally, the combination of ganetespib enhances the efficacy of PD-L1 antibody (STI-A1015) in syngeneic mouse models of CRC and melanoma.<sup>13</sup>

Herein, we demonstrate that this novel regimen was tolerable, with no new safety signals observed, when compared to prior studies in patients previously treated with pembrolizumab, or XL888 with the combination of Vemurafenib.<sup>11</sup> In this heavily pre-treated patient cohort, prolonged stable disease was observed in six patients (2 in escalation cohort and 4 in expansion cohort) with treatment refractory pMMR CRC. Importantly, the combination therapy did not demonstrate any new or unexpected toxicities. The severity or incidence of AEs did not differ from those previously reported for either agent alone.<sup>11</sup>

Our correlative studies validated that XL888 had biologic activity in patients. Namely, they demonstrated the addition of XL888, to a pembrolizumab regimen, elicited unique immunomodulatory effects in patient metastatic liver tumors and potent inflammatory effects in systemic circulation. This analysis employed several complementary methodologies, including mIHC, mass cytometry, and plasma cytokine profiling. Our mIHC analysis, even limited to a single post-treatment time point, showed tumors exposed to combination therapy had decreased IL6<sup>+</sup> cells and CD68<sup>+</sup> macrophages. These results were aligned with our prior pre-clinical observations that

XL888 reduces IL-6 production in vitro.<sup>12</sup> Although only feasible in a small cohort of patients due to sample limitations, CyTOF data highlighted unexpected decreases in circulating CD19<sup>+</sup> B cells and CD3<sup>+</sup> T lymphocytes. Despite constraints in cell abundance and tissue quality, affecting the analysis of CD4<sup>+</sup> and CD8<sup>+</sup> T cells, these findings suggest broad impacts of this treatment regimen systemically on PBMCs. Plasma cytokine profiles revealed increased levels of inflammatory cytokines, particularly in patients receiving the combination therapy, suggesting enhanced systemic immune activation.

While evidence of stable disease in treatment-refractory CRC patients is encouraging, we acknowledge the lack of responses in this heavily pre-treated population. Several factors may account for this. Our correlative data were particularly informative in understanding reasons for treatment resistance. First, T lymphocytes were sparse in the liver metastases. This finding was consistent regardless of the modality and reproducible using multiple complementary tissue-based and single-cell methodologies. In fact, in some tissues, CD4<sup>+</sup> or CD8<sup>+</sup> T cells were undetectable. Validating this overall absence of any T cell infiltrate is important information, as it represents an obvious barrier to efficacy from PD-1-targeted antibodies. This result also highlights a key ‘real-world’ differential immune feature that distinguishes patients with liver metastasis from pre-clinical murine models that may harbor more abundant T cells and are typically used to generate efficacy data in support of clinical trials. Indeed, liver metastases are known to possess mechanisms by which infiltrating CD8<sup>+</sup> T cells are decisively eliminated by tumor-associated macrophages via Fas-FasL-mediated apoptosis.<sup>24</sup> Second, it is also possible that Hsp90 inhibition could have elicited cell context-dependent mechanisms that complicated its intended anti-inflammatory action. For example, while our pre-clinical data point to a role for Hsp90i in dampening CAF-derived inflammatory cytokine production, these drugs may have unintended, on-target effects on other immune cells that

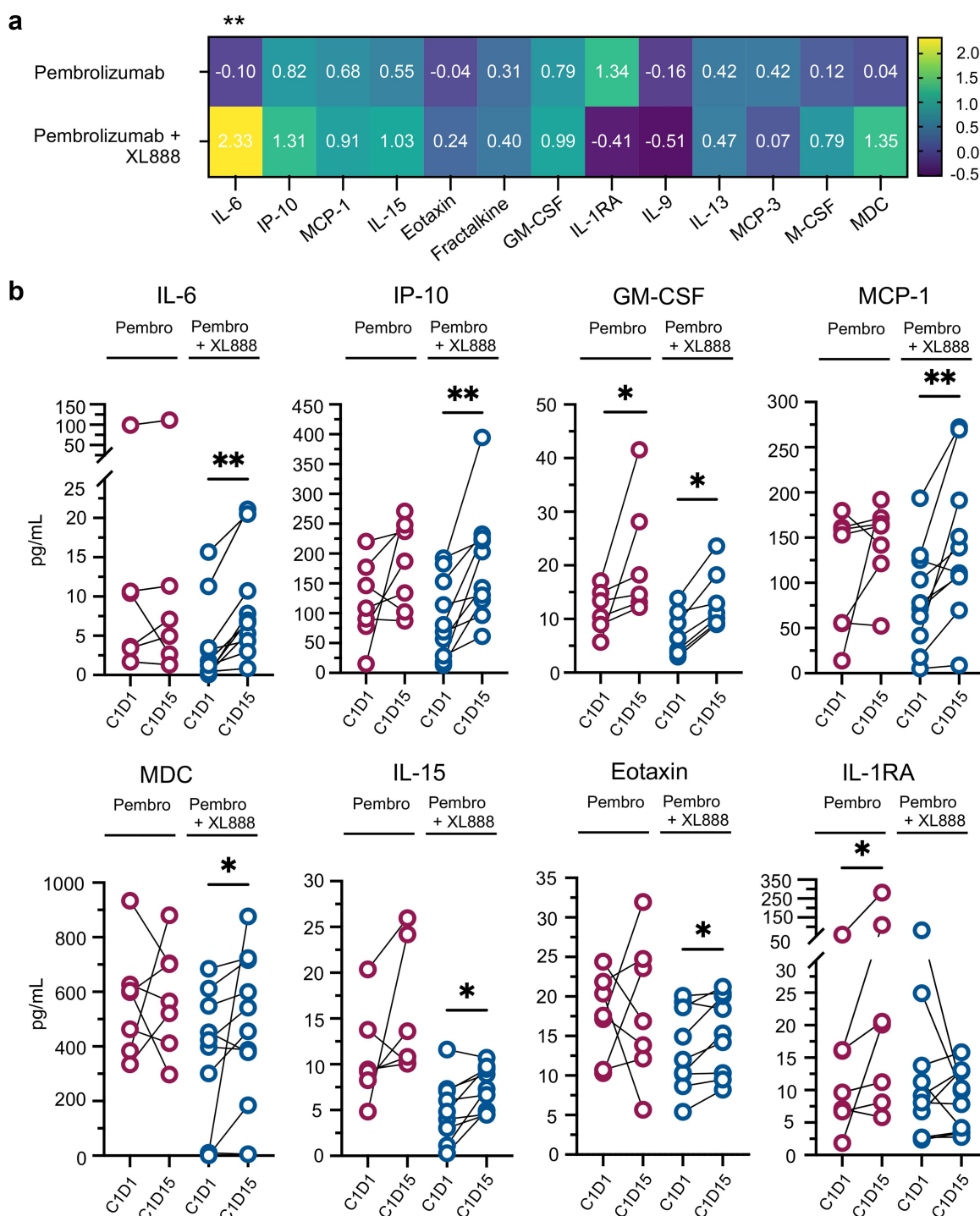


**Figure 5.** Differential plasma cytokine profiles in patients treated with pembrolizumab alone or in combination with XL888. (a) Heat map of plasma cytokine modulation in response to treatment. Relative fold change ( $\log_2$  transformed) of multiple cytokines, normalized to treatment baseline (C1D1) in patients receiving pembrolizumab alone (top panel) or in combination with XL888 (bottom panel). Mann–Whitney test was performed to compare cytokine levels between the two treatment groups at each time point, with statistical significance at  $**p < 0.01$ . (b) Quantitative analysis of cytokine concentrations in blood plasma for eight cytokines: IL-6 ( $p = 0.0020$ ), IP-10 ( $p = 0.0020$ ), GM-CSF ( $p = 0.0312$ ,  $0.0156$ ), MCP-1 ( $p = 0.0059$ ) (top, left to right), and MDC ( $p = 0.0488$ ), IL-15 ( $p = 0.0195$ ), Eotaxin ( $p = 0.0273$ ), IL-1RA ( $p = 0.132$ ) (bottom, left to right). Changes in biomarker levels from baseline (C1D1) to post-treatment (C1D15) were assessed using the Wilcoxon matched-pairs signed rank test, statistical significance at  $*p < 0.05$  and  $**p < 0.01$ .

concurrently dampen immune response. Other Hsp90i, such as geldanamycin, have also been shown to limit dendritic cell (DC) maturation and activation, which could in turn jeopardize antitumor T cell responses that depend on effective antigen presentation.<sup>12,25,26</sup> The frequency of cells harboring markers compatible with DC phenotypes (even in baseline

patient tumor biopsies) was also quite low in this study. A potential approach could involve introducing Hsp90i at an earlier stage of disease progression. This timing might be advantageous as there could be a higher presence of T cells and dendritic cells within the TME during earlier disease stages.

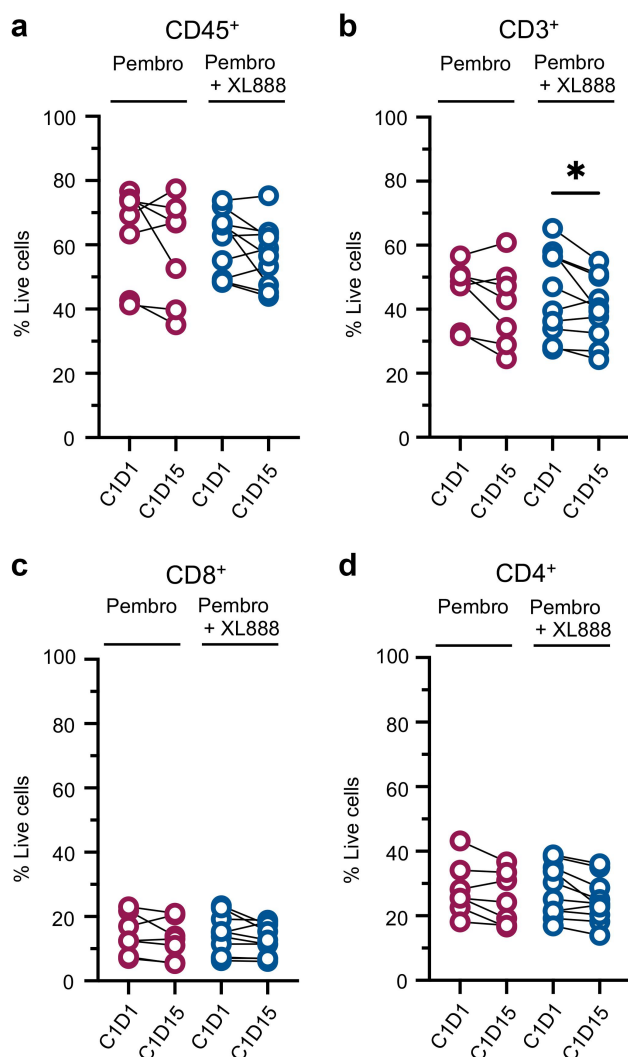


**Figure 6.** CyTOF-based immune profiling reveals alterations in peripheral blood immune cell subsets. a-d. The percentage of live cells expressing CD45<sup>+</sup> (a), CD3<sup>+</sup> (b), CD8<sup>+</sup> (c), and CD4<sup>+</sup> (d) Changes in immune cell populations from C1D1 to C1D15 were assessed using the Wilcoxon matched-pairs signed rank test with statistical significance set at  $p < 0.05$ .

Like many early phase clinical trials, this study faced limitations that may affect the interpretation of the results. The limited number of T cells available for analysis in the samples likely constrained the efficacy of this combination and restrains the depth of our immune correlative studies, such as CyTOF and multiplex IHC. We also acknowledge the heterogeneity of tumors and use of core needle biopsies may not capture the full diversity of the tumor microenvironment, potentially skewing our understanding of immune interactions within the tumors. Additionally, the CRC liver biopsies revealed a scarcity of CAFs, which are known for their high heterogeneity in patient tumors, potentially explaining the discrepancy between pre-clinical studies and our trial findings.<sup>27,28</sup> Furthermore, the inherent genetic variability among human CRC cases could influence the data, as genetic differences among tumors can affect their immune profiles and response to treatments. Together these factors underscore the need for cautious interpretation of our findings and their application to larger, more diverse cohorts of CRC patients.

Despite limited efficacy beyond stable disease in patients receiving pembrolizumab and XL888, our findings suggest avenues for further investigation. Future studies should explore alternative combinations, particularly how Hsp90i may modulate other immune checkpoint inhibitors, as it can downregulate PD-L1 at physiological doses.<sup>29</sup> The lack of positive outcomes may relate to immune system changes, tumor biology, or metastatic site differences. For instance, a trial combining a Hsp90i with nivolumab showed a 0% overall response rate (ORR) in liver metastases versus 13% in lung metastases.<sup>30</sup> Interestingly, one patient with lung metastases in our trial had prolonged stable disease, indicating that immune landscape variations across metastatic sites may influence responses. Lung metastases tend to have higher T cell infiltration and less immunosuppression, compared to liver metastases, which are characterized by T regulatory and macrophage-mediated immune suppression.<sup>24,31–33</sup> Thus, elevated T cell infiltration may render metastatic lung lesions more responsive to immunotherapies in comparison to liver lesions. Research could target this combination in patients with specific metastatic profiles, especially lung metastases. Additionally, investigating the regimen in patients with higher baseline T cell levels or combining it with agents that enhance T cell activity may yield better results. Integrating this approach with earlier therapies like chemotherapy or radiotherapy could improve efficacy against the immune suppressive tumor microenvironment in advanced colorectal cancer. This study provides a comprehensive evaluation of the combination of pembrolizumab and XL888, laying the groundwork for future studies to build upon.

## Acknowledgments

Research reported in this publication was supported by the shared resources and cores at Winship Cancer Institute and Emory University including the Winship Cancer Tissue Pathology Shared Resource, the Winship Immune Monitoring Shared Resource, the Winship Data Shared Resource, and the Winship Biostatistics Shared Resource under NIH/NCI award number P30CA138292. The content is solely the responsibility of the authors and does not necessarily represent the official views of the National Institutes of Health. Figure schematics were created with BioRender.com.

## Disclosure statement

OBA has consulted for Ipsen Pharmaceuticals, Aadi Bioscience, Taiho, Pfizer, Seagen Inc., Bristol-Myers Squibb (BMS), and AstraZeneca (AZ). OBA has received research funding from Taiho Oncology, Ipsen Pharmaceuticals, GSK, BMS, PCI Biotech AS, ASCO, Calithera Biosciences, Inc., SynCore Biotechnology Co. Ltd., Suzhou Transcenta Therapeutics Co., Ltd, Corcept Therapeutics Inc., Hutchison MediPharma, Boehringer Ingelheim, Xencor Inc., Cue Biopharma, Inc., Merck, Syros Pharmaceuticals Inc., Inhibitex Inc, Arcus Biosciences Inc. and ImmunoGen. OBG has received funding from Genentech, Inc. through a sponsored research agreement with Emory University. MD has consulted for Novartis and Guardant Health. CJH is employed by Eli Lilly, Inc. CMP has received research funding through a sponsored research agreement between the Medical University of South Carolina and Obsidian, Lycera, and ThermoFisher, and is the cofounder of Ares Immunotherapy. BER has consulted for AZ, Ipsen, Exelixis, Seagen and

received research funding from BMS, Merck, AZ, Novartis, EUSA, adaptimmune, Bayer, Exelixis. GBL has consulted for ProDa Biotech, LLC and received compensation. GBL has received research funding through a sponsored research agreement between Emory University and Merck and Co., BMS, Boehringer-Ingelheim, and Vaccinex. The remaining authors have no conflicts of interest to disclose.

## Funding

This work was supported by the National Institutes of Health [P30CA138292, R01CA228406, R21CA266088].

## Data availability statement

The data that support the findings of this study are available from the corresponding author, GBL, upon reasonable request.

## References

1. Siegel RL, Miller KD, Wagle NS, Jemal A. Cancer statistics, 2023. *CA Cancer J Clin.* 2023 Jan. 73(1):17–48. doi:10.3322/caac.21763.
2. Rahib L, Wehner MR, Matrisian LM, Nead KT. Estimated projection of US cancer incidence and death to 2040. *JAMA Netw Open.* 2021 Apr 1. 4(4):e214708. doi:10.1001/jamanetworkopen.2021.4708.
3. Sargent D, Sobrero A, Grothey A, O'Connell MJ, Buyse M, Andre T, Zheng Y, Green E, Labianca R, O'Callaghan C, et al. Evidence for cure by adjuvant therapy in colon cancer: observations based on individual patient data from 20,898 patients on 18 randomized trials. *J Clin Oncol.* 2009 Feb 20. 27(6):872–877. doi:10.1200/JCO.2008.19.5362.
4. Adam R, Bhangui P, Poston G, Mirza D, Nuzzo G, Barroso E, Ijzermans J, Hubert C, Ruers T, Capussotti L, et al. Is perioperative chemotherapy useful for solitary, metachronous, colorectal liver metastases? *Ann Surg.* 2010 Nov. 252(5):774–787. doi:10.1097/SLA.0b013e3181fc3e3.
5. Siegel RL, Miller KD, Fuchs HE, Jemal A. Cancer statistics, 2022. *CA Cancer J Clin.* 2022 Jan. 72(1):7–33. doi:10.3322/caac.21708.
6. Amodio V, Mauri G, Reilly NM, Sartore-Bianchi A, Siena S, Bardelli A, Germano G. Mechanisms of immune escape and resistance to checkpoint inhibitor therapies in mismatch repair deficient metastatic colorectal cancers. *Cancers (Basel).* 2021 May 27. 13(11):2638. doi:10.3390/cancers13112638.
7. Andre T, Shiu KK, Kim TW, Jensen BV, Jensen LH, Punt C, Smith D, Garcia-Carbonero R, Benavides M, Gibbs P, et al. Pembrolizumab in microsatellite-Instability–High advanced colorectal cancer. *N Engl J Med.* 2020 Dec 3. 383(23):2207–2218. doi:10.1056/NEJMoa2017699.
8. Bullock AJ, Schlechter BL, Fakih MG, Tsimberidou AM, Grossman JE, Gordon MS, Wilky BA, Pimentel A, Mahadevan D, Balmanoukian AS, et al. Botensilimab plus balstilimab in relapsed/refractory microsatellite stable metastatic colorectal cancer: a phase 1 trial. *Nat Med.* Jun 13 2024;2024;30(9):2558–2567. doi:10.1038/s41591-024-03083-7.
9. Whitesell L, Lindquist SL. HSP90 and the chaperoning of cancer. *Nat Rev Cancer.* 2005 Oct. 5(10):761–772. doi:10.1038/nrc1716.
10. Kim YS, Alarcon SV, Lee S, Lee M-J, Giaccone G, Neckers L, Trepel J. Update on Hsp90 inhibitors in clinical trial. *Curr Top Med Chem.* 2009;9(15):1479–1492. doi:10.2174/156802609789895728.
11. Eroglu Z, Chen YA, Gibney GT, Weber JS, Kudchadkar RR, Khushalani NI, Markowitz J, Brohl AS, Tetteh LF, Ramadan H, et al. Combined BRAF and HSP90 inhibition in patients with unresectable BRAF V600E-Mutant melanoma. *Clin Cancer Res.* 2018 Nov 15. 24(22):5516–5524. doi:10.1158/1078-0432.CCR-18-0565.
12. Zhang Y, Ware MB, Zaidi MY, Ruggieri AN, Olson BM, Komar H, Farren MR, Nagaraju GP, Zhang C, Chen Z, et al. Heat shock protein-90 inhibition alters activation of pancreatic stellate cells and enhances the efficacy of PD-1 blockade in pancreatic cancer. *Mol Cancer Ther.* 2021 Jan. 20(1):150–160. doi:10.1158/1535-7163.Mct-19-0911.
13. Proia DA, Kaufmann GF. Targeting heat-shock protein 90 (HSP90) as a complementary strategy to immune checkpoint blockade for cancer therapy. *Cancer Immunol Res.* 2015 June. 3(6):583–589. doi:10.1158/2326-6066.CIR-15-0057.
14. Noman MZ, Desantis G, Janji B, Hasmim M, Karray S, Dessen P, Bronte V, Chouaib S. PD-L1 is a novel direct target of HIF-1 $\alpha$ , and its blockade under hypoxia enhanced MDSC-mediated T cell activation. *J Exp Med.* 2014 May 5. 211(5):781–790. doi:10.1084/jem.20131916.
15. Bellucci R, Martin A, Bommarito D, Wang K, Hansen SH, Freeman GJ, Ritz J. Interferon- $\gamma$ -induced activation of JAK1 and JAK2 suppresses tumor cell susceptibility to NK cells through upregulation of PD-L1 expression. *Oncoimmunology.* 2015 June. 4(6):e1008824. doi:10.1080/2162402X.2015.1008824.
16. Seo SK, Seo DI, Park WS, Jung W-K, Lee D-S, Park S-G, Choi JS, Kang M-S, Choi YH, Choi I, et al. Attenuation of ifn- $\gamma$ -induced B7-H1 expression by 15-deoxy- $\delta$ 12,14-prostaglandin J2 via down-regulation of the Jak/STAT/IRF-1 signaling pathway. *Life Sci.* 2014 Sep 1. 112(1–2):82–89. doi:10.1016/j.lfs.2014.07.021.
17. Nagaraju GP, Park W, Wen J, Mahaseth H, Landry J, Farris AB, Willingham F, Sullivan PS, Proia DA, El-Hariry I, et al. Erratum to: antiangiogenic effects of ganetespib in colorectal cancer mediated through inhibition of HIF-1 $\alpha$  and STAT-3. *Angiogenesis.* 2013 Oct. 16(4):903–917. doi:10.1007/s10456-013-9364-7.
18. McCaw ZR, Tian L, Wei LJ. Appropriate analysis of duration of response data in cancer trials. *JAMA Oncol.* 2020 Dec 1. 6(12):1978. doi:10.1001/jamaoncol.2020.4657.
19. Huang B, Tian L, Talukder E, Rothenberg M, Kim DH, Wei LJ. Evaluating treatment effect based on duration of response for a comparative oncology study. *JAMA Oncol.* 2018 June 1. 4(6):874–876. doi:10.1001/jamaoncol.2018.0275.
20. Bankhead P, Loughrey MB, Fernández JA, Dombrowski Y, McArt DG, Dunne PD, McQuaid S, Gray RT, Murray LJ, Coleman HG, et al. QuPath: open source software for digital pathology image analysis. *Sci Rep.* 2017 Dec 4. 7(1):16878. doi:10.1038/s41598-017-17204-5.
21. Nagaraju GP, Long TE, Park W, Landry JC, Taliaferro-Smith L, Farris AB, Diaz R, El-Rayes BF. Heat shock protein 90 promotes epithelial to mesenchymal transition, invasion, and migration in colorectal cancer. *Mol Carcinog.* 2015 Oct. 54(10):1147–1158. doi:10.1002/mc.22185.
22. Nagaraju GP, Alese OB, Landry J, Diaz R, El-Rayes BF. HSP90 inhibition downregulates thymidylate synthase and sensitizes colorectal cancer cell lines to the effect of 5FU-based chemotherapy. *Oncotarget.* 2014 Oct 30. 5(20):9980–9991. doi:10.18632/oncotarget.2484.
23. Schulz R, Moll UM. Targeting the heat shock protein 90: a rational way to inhibit macrophage migration inhibitory factor function in cancer. *Curr Opin Oncol.* 2014 Jan. 26(1):108–113. doi:10.1097/CCO.000000000000036.
24. Yu J, Green MD, Li S, Sun Y, Journey SN, Choi JE, Rizvi SM, Qin A, Waninger JJ, Lang X, et al. Liver metastasis restrains immunotherapy efficacy via macrophage-mediated T cell elimination. *Nat Med.* 2021 Jan. 27(1):152–164. doi:10.1038/s41591-020-1131-x.
25. Trojandt S, Reske-Kunz AB, Bros M. Geldanamycin-mediated inhibition of heat shock protein 90 partially activates dendritic cells, but interferes with their full maturation, accompanied by impaired upregulation of RelB. *J Exp Clin Cancer Res.* 2014 Feb 13. 33(1):16. doi:10.1186/1756-9666-33-16.
26. Bae J, Mitsiades C, Tai YT, Bertheau R, Shammam M, Batchu, R.B, Li, C, Catley, L, Prabhala, R, Anderson, K.C, et al. Phenotypic and functional effects of heat shock protein inhibition on dendritic cell. *J Immunol.* [2007 June 15]. 178(12):7730–7737. doi:10.4049/jimmunol.178.12.7730.
27. Pan X, Zhou J, Xiao Q, Fujiwara K, Zhang M, Mo G, Gong W, Zheng L. Cancer-associated fibroblast heterogeneity is associated

- with organ-specific metastasis in pancreatic ductal adenocarcinoma. *J Hematol Oncol.* **2021** Nov 2. 14(1):184. doi:[10.1186/s13045-021-01203-1](https://doi.org/10.1186/s13045-021-01203-1).
28. Sullivan L, Pacheco RR, Kmeid M, Chen A, Lee H. Tumor stroma ratio and its significance in locally advanced colorectal cancer. *Curr Oncol.* **2022** May 3. 29(5):3232–3241. doi:[10.3390/curroncol29050263](https://doi.org/10.3390/curroncol29050263).
  29. Zavareh RB, Spangenberg SH, Woods A, Martínez-Peña F, Lairson LL. HSP90 inhibition enhances cancer immunotherapy by modulating the surface expression of multiple immune checkpoint proteins. *Cell Chem Biol.* **2021** Feb 18. 28(2):158–168.e5. doi:[10.1016/j.chembiol.2020.10.005](https://doi.org/10.1016/j.chembiol.2020.10.005).
  30. Kawazoe A, Itahashi K, Yamamoto N, Kotani D, Kuboki Y, Taniguchi H, Harano K, Naito Y, Suzuki M, Fukutani M, et al. TAS-116 (pimitepib), an oral HSP90 inhibitor, in combination with nivolumab in patients with colorectal cancer and other solid tumors: an open-label, Dose-Finding, and expansion phase Ib trial (EPOC1704). *Clin Cancer Res.* [2021 Dec 15]. 27(24):6709–6715. doi:[10.1158/1078-0432.Ccr-21-1929](https://doi.org/10.1158/1078-0432.Ccr-21-1929).
  31. García-Mulero S, Alonso MH, Pardo J, Santos C, Sanjuan X, Salazar R, Moreno V, Piulats JM, Sanz-Pamplona R. Lung metastases share common immune features regardless of primary tumor origin. *J Immunother Cancer.* **2020** June. 8(1):e000491. doi:[10.1136/jitc-2019-000491](https://doi.org/10.1136/jitc-2019-000491).
  32. Choi MG, Choi CM, Lee DH, Kim S-W, Yoon S, Kim WS, Ji W, Lee JC. Different prognostic implications of hepatic metastasis according to front-line treatment in non-small cell lung cancer: a real-world retrospective study. *Transl Lung Cancer Res.* **2021** June. 10(6):2551–2561. doi:[10.21037/tlcr-21-206](https://doi.org/10.21037/tlcr-21-206).
  33. Lee JC, Mehdizadeh S, Smith J, Young A, Mufazalov IA, Mowery CT, Daud A, Bluestone JA. Regulatory T cell control of systemic immunity and immunotherapy response in liver metastasis. *Sci Immunol.* **2020** Oct 2. 5(52). doi:[10.1126/sciimmunol.aba0759](https://doi.org/10.1126/sciimmunol.aba0759).
  34. Polley DJ, Latham P, Choi MY, Buhler KA, Fritzler MJ, Fritzler ML. Identification of novel clusters of co-expressing cytokines in a diagnostic cytokine multiplex test. *Front Immunol.* **2023**;14:1223817. doi:[10.3389/fimmu.2023.1223817](https://doi.org/10.3389/fimmu.2023.1223817).
  35. Lim SY, Lee JH, Gide TN, Menzies AM, Guminski A, Carlino MS, Breen EJ, Yang JYH, Ghazanfar S, Kefford RF, et al. Circulating cytokines predict immune-related toxicity in melanoma patients receiving anti-PD-1-Based immunotherapy. *Clin Cancer Res.* **2019** Mar 1. 25(5):1557–1563. doi:[10.1158/1078-0432.Ccr-18-2795](https://doi.org/10.1158/1078-0432.Ccr-18-2795).
  36. Bagwell CB, Hunsberger B, Hill B, Herbert D, Bray C, Selvanantham T, Li S, Villasboas JC, Pavelko K, Strausbauch M, et al. Multi-site reproducibility of a human immunophenotyping assay in whole blood and peripheral blood mononuclear cells preparations using CyTOF technology coupled with Maxpar Pathsetter, an automated data analysis system. *Cytometry B Clin Cytom.* **2020** Mar. 98(2):146–160. doi:[10.1002/cyto.b.21858](https://doi.org/10.1002/cyto.b.21858).

## Appendices 1-5: Extended materials and methods

### Appendix 1. Metastatic liver multiplex immunohistochemistry (mIHC) and analysis

Tissue biopsies were fixed in 10% buffered formalin phosphate (catalog# SF100-4, Fisher Scientific) and embedded in paraffin. Sections of 4  $\mu$ m thickness were cut using a rotary microtome and mounted onto positively charged slides (catalog # 10200WH, Path Supply) in a 40°C dH<sub>2</sub>O bath. After mounting, slides were incubated at 60°C for 1 hr to facilitate water evaporation. The automated multiplex immunohistochemistry (mIHC) staining protocol was executed using the DISCOVERY ULTRA autostainer (Roche Diagnostics). To begin, slides were warmed to 69°C for 8 min for deparaffinization, followed by three cycles using 10X EZ-Prep solution (catalog# 0527977100, DISCOVERY). Heat-induced epitope retrieval (HIER) was completed at room temperature for 20 min using ethylenediaminetetraacetic acid solution (EDTA) (catalog# E8008-100 ML, Millipore). To block endogenous peroxidase activity, DISCOVERY Inhibitor (catalog# 7017944001, Roche) was applied prior to antigen staining. The staining protocol accommodates a maximum of six primary antibodies, incubated for 40 min each and diluted using Diamond: Antibody Diluent (catalog# 938B-09, Cell Marque). Two distinct staining panels were utilized (Supplementary Table S1). Through a sequence of incubations, panel 1 targeted the following markers:  $\alpha$ SMA, CD3, CD19, CD68, IL6, and CK19. Panel 2 focused on the following markers: CD4, CD8, CK-19, FoxP3, ROR $\gamma$ t, and T-bet. Next, OmniMap HRP secondary antibodies (catalog# 05269652001- $\alpha$ -mouse or # 05269679001- $\alpha$ -rabbit, Roche) were incubated for 12 min. Additionally, Opal™ tyramide signal amplification fluorophores (listed in Supplementary Table S1, Akoya Biosystems) were diluted using 1X Amplification Diluent (catalog# FP1609, Akoya Biosystems) or Disc. Diluent P.S.S., specifically for Opal 780 (catalog# 05266815001, Akoya Biosystems), applied, and incubated for 16 min. A denaturation cycle was then initiated using high heat (93°C) and Cell Conditioner 2 (catalog# 05279798001, Roche) for 8 min. Slides were counterstained with Spectral DAPI (catalog# FP1490, Akoya Biosystems) and incubated for 16 min. After completing the staining process, slides were rinsed briefly in a detergent solution to remove any liquid coverslip residue and then cover-slipped using Vectashield® Antifade mounting medium (catalog# H-1000-10, Vector Laboratories). Slides were cured in darkness for 24 h at 4°C before imaging with the Vectra® Polaris™ Automated Quantitative Pathology Imaging System, with ideal exposures determined by averaging across multiple slides using the Vectra Polaris software. One out of the eight patients' biopsy cores (pembrolizumab) were unsuitable for mIHC analysis due to insufficient tissue quantity and inadequate staining.

The cured slides with fluorescently labeled tissue sections were subjected to whole-slide scanning and subsequent analysis utilizing QuPath v0.4.4.4 (University of Edinburgh, Edinburgh, Scotland, UK)<sup>20</sup>. Cell segmentation was performed using the DAPI channel (C1) with specific settings: 0.4967  $\mu$ m pixel size, 6.0  $\mu$ m background radius, background by reconstruction method, 1.0  $\mu$ m median filter radius, 0.5  $\mu$ m sigma size, 3.0  $\mu$ m<sup>2</sup> minimum area, 400  $\mu$ m<sup>2</sup> maximum area, and a threshold of 5, with a 4.0  $\mu$ m cell expansion area. Following cell detection, a publicly available script (accessible at <https://www.imagescientist.com/creating-a-classifier>) was adapted for the classification of cells. Threshold values for each fluorescent channel were determined by applying defined visual cutoffs (fluorescent intensity ratio) to ascertain the count of positive cells for individual fluorescent signal intensities or combinations thereof. Batch mode in the script editor facilitated simultaneous analysis of all whole-image sections. Subsequently, data was exported for further analysis using Microsoft Excel (V.16.80) and GraphPad Prism (V.9.4.1) tools. Cellular percentages were calculated by dividing the total cell detections for each fluorescent signal or combination of signals by the overall number of cell detections. Spatial analysis was used to study distribution patterns of immune and stromal cell populations relative to the metastatic tumor margin and the stromal compartment. For this analysis, the x and y coordinates of phenotyped cells were extracted from whole tissue images. Next, these coordinates were used to map tissue and evaluate spatial organization of tissue

(Supplementary Figure S2A-B). Using the SPIAT package in R (PMID: 37188662), tissue architecture was annotated according to cancer cell (CK19+) density into four areas: tumor, internal margin, external margin, stroma, with stromal compartment located farthest away from cancer cells.

### Appendix 2. Mechanical and enzymatic dissociation of metastatic liver tissue

Fresh metastatic liver tissue cores were subjected to both a mechanical and enzymatic dissociation process utilizing the gentleMACS Dissociator (catalog# 130-093-235, Miltenyi Biotec). Tissue cores were cut into small portions (2–3 mm), via scalpel, and placed into the gentleMACS™ C-tubes (catalog# 130-093-237, Miltenyi Biotec) containing digestion media—RPMI 1640 and enzymes H, R, and A (Miltenyi Biotec) according to the manufacturer's protocol. C-tubes containing the liver biopsy core and digestion media were secured in the gentleMACS dissociator and the mechanical dissociation program, h\_tumor\_01, was run for two cycles at 37 sec each. Samples were then placed in a 37°C incubator shaker for 30 min, again followed by 2 cycles of dissociation, then placed back into the 37°C incubator shaker for an additional 30 min. The dissociated digestion mixture was transferred through a 70  $\mu$ m filter and centrifuged at 500  $\times$  g for 5 min, resuspended and washed in 1 $\times$  PBS, and then centrifuged again yielding approximately 2  $\times$  10<sup>6</sup> cells or less per sample for CyTOF analysis.

### Appendix 3. Single-cell mass cytometry (CyTOF) staining and analysis of metastatic liver tissue

Cells from the dissociated metastatic liver tissue were resuspended with 1 mL of 1X PBS containing Cell-ID™ Cisplatin (catalog # 201064, Standard BioTools) for viability staining. Viability staining was neutralized using the Maxpar® Cell Staining Buffer and cells were washed two more times with the Maxpar® Cell Staining Buffer in preparation for surface and intracellular staining (Supplementary Table S2). After the surface stain incubation, cells were washed with buffer and fixed with 1.6% formaldehyde (FA) solution. After permeabilization, cells were stained for intracellular markers. Cells were washed with buffer twice, stained with Cell-ID™ Intercalator-Ir—125  $\mu$ m (catalog# 201192A, Standard BioTools), and samples acquired on a Helios mass cytometer followed by normalization via CyTOF software algorithms.

The Flowjo V10.8.1 and Cytobank software were used to analyze normalized CyTOF FCS files. Based on the Standard BioTool's technical notation and clean up strategy (PN 400248 B1), FSC files were manually cleaned. Samples with a minimum of 250 live cells (DNA2+) were eligible for further analysis (pembrolizumab n = 4; pembrolizumab & XL888 n = 4). Cleaned FCS files were exported from Flowjo as individual sample files.

### Appendix 4. Plasma cytokine analysis

Peripheral blood specimens were collected in EDTA tubes at C1D1 and C1D15 of treatment. Notably, one patient was excluded from the analyses due to the absence of a blood draw at C1D15. Specimens were maintained at room temperature, processed within 24 h of blood draw, and centrifuged at 450  $\times$  g for 10 min to isolate plasma from whole blood. Patient plasma samples were kept undiluted and frozen at -80°C for subsequent profiling utilizing the Human Cytokine/Chemokine Panel, a 48-plex Discovery Assay™ Array (catalog # HD48A; Eve Technologies), with details of specific analytes observed available in Supplementary Table 3. The array employs Luminex™ laser bead technology, a well-established and highly sensitive bead-based multiplex assay for quantifying analytes.<sup>34,35</sup> Each plasma sample was analyzed in its undiluted state and in duplicate, undergoing assessment for final observed concentrations in pg/mL. These concentrations were derived

by averaging the duplicate plasma measurements, which alongside a standard curve, reflected the median fluorescence intensity (FI) value of the bead population for each specific analyte.

## **Appendix 5. Whole blood MaxPar™ Direct Immune Profiling Assay (MDIPA)**

After separation of plasma from whole blood, samples underwent Ficoll® (catalog# GE17-1440-02, Millipore) density gradient centrifugation at  $800 \times g$  for 30 min to separate peripheral blood

mononuclear cells (PBMCs). After separation, PBMCs were washed once with  $1\times$  PBS and subsequently cryopreserved in Serum-Free Cell Freezing Medium containing DMSO (catalog # C6295-50 mL, Sigma-Aldrich). Samples were acquired utilizing a Helios mass cytometer (part number 107002; Standard Biotoools) and raw FCS files were normalized using the built-in normalizer algorithm within the CyTOF software. Comprehensive analysis of immune cell populations was done using MDIPA as per manufacturer's protocol (Standard Biotoools).<sup>36</sup> Supplementary Table 4 outlines the cellular markers identified on the surface of PBMCs. Normalized FCS were analyzed using the Maxpar PathSetter software version 2.0.45.